Paul B. Chang
Sibley School of Mechanical and Aerospace Engineering, Cornell University, Ithaca, NY 14853

Brian J. Williams
Department of Statistics, The Ohio State University, Columbus, OH 43210

Kanwaljeet Singh Bawa Bhalla

Thomas W. Belknap

Sibley School of Mechanical and Aerospace Engineering, Cornell University, Ithaca, NY 14853

Thomas J. Santner

William I. Notz

Department of Statistics, The Ohio State University, Columbus, OH 43210

Donald L. Bartel
Sibley School of Mechanical and Aerospace Engineering, Cornell University, Ithaca, NY 14853

Design and Analysis of Robust Total Joint Replacements: Finite Element Model Experiments With Environmental Variables

Computer simulations of orthopaedic devices can be prohibitively time consuming, particularly when assessing multiple design and environmental factors. Chang et al. (1999) address these computational challenges using an efficient statistical predictor to optimize a flexible hip implant, defined by a midstem reduction, subjected to multiple environmental conditions. Here, we extend this methodology by: (1) explicitly considering constraint equations in the optimization formulation, (2) showing that the optimal design for one environmental distribution is robust to alternate distributions, and (3) illustrating a sensitivity analysis technique to determine influential design and environmental factors. A thin midstem diameter with a short stabilizing distal tip minimized the bone remodeling signal while maintaining satisfactory stability. Hip joint force orientation was more influential than the effect of the controllable design variables on bone remodeling and the cancellous bone elastic modulus had the most influence on relative motion, both results indicating the importance of including uncontrollable environmental factors. The optimal search indicated that only 16 to 22 computer simulations were necessary to predict the optimal design, a significant savings over traditional search techniques.
[DOI: 10.1115/1.1372701]

Introduction

Orthopaedic implants are required to sustain many years of demanding activity. However, unlike most products, these devices cannot be easily repaired or tuned because they reside in the body. Therefore, a successful design must be robust with respect to unpredictable loads and changing environments. This philosophy must be reflected in the computer simulations used to design implants.

Several authors [1–5] have determined optimally shaped hip implants subjected to a limited set of typical gait loads and bone properties. However, it is reasonable to question whether the same implants would perform well, for example, subject to the large torsional moments generated during stair ascent [6,7]. Similarly, femur geometry varies both across a patient population [8] and over time within the same patient. The referenced studies were not limited by the biomechanical concepts but rather by computational challenges. Traditional optimization techniques are iterative and time consuming. As a result, it becomes impractical to consider a comprehensive set of environmental conditions.

In a previous study [9], a statistical methodology was introduced to search efficiently for designs that perform optimally in the presence of environmental variations such as loading conditions and varying bone properties. This new approach produces specific choices for the design variables that also account for variability in the environment. The new approach requires far fewer evaluations of the response than traditional direct-search techniques. The method was demonstrated with an example of a femoral component design for total hip arthroplasty. Computationally simple two-dimensional models were used to confirm the effectiveness of the statistical method for finding the optimal designs. The results indicated that the method was appropriate for use with more complex computer models.

In the present study, a three-dimensional nonlinear finite element model was used to predict the structural response. We conducted parallel physical experiments to validate the optimal design predicted using the computer experiments. Several important aspects of the statistical methods are addressed here that were not previously discussed. These include: (1) inclusion of constraint equations, (2) robustness of optimal designs with respect to alternate environmental variable distributions, and (3) sensitivity analysis to identify influential variables, a useful tool for both surgeons and design engineers.

Methods

Optimization Formulation. The response, $Y(\mathbf{x_d},\mathbf{x_e})$, is a function of the design variables, $\mathbf{x_d}$, and environmental variables, $\mathbf{x_e}$. The objective function, $L(\mathbf{x_d})$, is obtained by averaging the

Contributed by the Bioengineering Division for publication in the JOURNAL OF BIOMECHANICAL ENGINEERING. Manuscript received by the Bioengineering Division January 23, 2000; revised manuscript received January 11, 2001. Associate Editor: T. M. Keaveny.

response, $Y(\mathbf{x_d},\mathbf{x_e})$, over a suitable probability distribution, $\mathbf{g}(\mathbf{x_e})$, of the environmental variables. The distribution incorporates variation in the patient population and modeling uncertainties. Assuming a suitable domain for $\mathbf{x_d}$, the optimization formulation is:

$$\text{Minimize:} \quad L(\mathbf{x_d}) = \int_{-\infty}^{\infty} Y(\mathbf{x_d},\mathbf{x_e})\mathbf{g}(\mathbf{x_e})d\mathbf{x_e} \tag{1}$$

$$\text{Subject to:} \quad \mathbf{h}(\mathbf{x_d}) = \mathbf{0} \ \text{ or } \ \mathbf{h}(\mathbf{x_d}) \leqslant \mathbf{0} \tag{2}$$

The constraint equations, $\mathbf{h}(\mathbf{x_d})$, have been explicitly incorporated into the formulation.

Overview. The general procedure was described previously in detail [9]. Here, we provide a summary. The finite element models used to compute the true structural response at a given set of input values are sufficiently complicated that several hours of CPU time are required for each run. This precludes the use of traditional numerical optimization techniques to solve Eq. (1) and (2). Instead, the procedure used is based on determining a computationally inexpensive predictor, $\hat{Y}(\mathbf{x_d},\mathbf{x_e})$, of the true response $Y(\mathbf{x_d},\mathbf{x_e})$. The predictor is based on the computed response at a small set of ''training'' sites. The training sites are chosen using a three-stage procedure described below. Once the predictor is determined, the predicted objective function, $\hat{L}(\mathbf{x_d})$, can be quickly determined by integration of the analytical expression $\hat{Y}(\mathbf{x_d},\mathbf{x_e})$ from Eq. (1) and an optimal solution based on $\hat{L}(\mathbf{x_d})$ is computed using traditional sequential search techniques. The constraint function, $\mathbf{h}(\mathbf{x_d})$, is itself an integral of a second computed response of $\mathbf{x_d}$ and $\mathbf{x_e}$. It is predicted using the same techniques that produce $\hat{L}(\mathbf{x_d})$. The optimal design minimizes the predicted objective function $\hat{L}(\mathbf{x_d})$ (within the control variable space) and satisfies the predicted constraints.

Training Sites. Training sites are locations in the design and environmental variable space where the responses $\mathbf{Y}(\mathbf{x_d},\mathbf{x_e})$ are calculated and subsequently used to develop a statistical predictor of the response at unsampled input sites. The training sites were chosen according to a three-stage sequential process similar to that of Bernardo et al. [10]. The first stage contained 8 points, the second stage 8 additional points, and the third stage 6 additional points for a total of 22 points ultimately used to train the predictor. The first stage design was chosen to be a Latin hypercube sample [11] that maximized the minimum inter-point distance because such designs tend to be spread throughout the variable space. The location of the minimizing $\mathbf{x_d}$ for the fitted model at each stage determined the Latin hypercube sampling area for the subsequent stage.

Response Predictor. We used an empirical best linear unbiased predictor (EBLUP) of $Y(\mathbf{x_d},\mathbf{x_e})$, denoted by $\hat{Y}(\mathbf{x_d},\mathbf{x_e})$. The description of $\hat{Y}(\mathbf{x_d},\mathbf{x_e})$ is given in Chang et al. [9] and is computed using the software GaSP[1] (Gaussian Stochastic Process). See Sacks et al. [12] and Stein [13] for additional details regarding best linear unbiased prediction.

Sensitivity Analysis. Broadly, sensitivity analysis is the assessment of the influence of each input variable on the response Y. A variable screening procedure introduced by Welch et al. [14] evaluates the effect of each input through calculation of main effects and interaction effects analogous to ANOVA. An estimate of each input's impact on total variation in the response can be made as well. Variables that have a higher contribution to this total variation have more influence on the response. Details regarding the partitioning of total variation into main effect and interaction effect components can be found in Jones et al. [15].

[1]GaSP was developed by Professor W. J. Welch, Department of Statistics and Actuarial Sciences, University of Waterloo, Ontario, Canada.

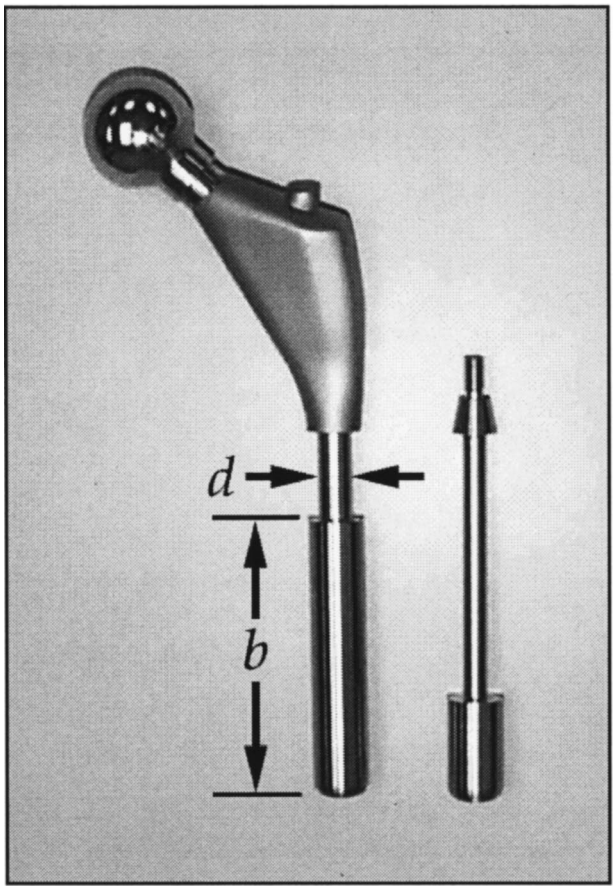

Fig. 1 Reduced midstem implant design. The implant design comprised a cementless cobalt chrome Ranawat–Burstein implant proximal geometry (Biomet, Inc., Warsaw IN) with a retrofitted 16 mm diameter, 100 mm long distal stem. Two example (b,d) configurations are shown. Nine distal stems were constructed for use in the physical experiment corresponding to all combinations of $b=\{25,50,75\}$ mm and $d=\{7,10,13\}$ mm. Finite element models of this geometry were constructed in which (b,d) could assume a continuous set of values.

Example. The example introduced in Chang et al. [9], involving the design of more flexible intramedullary stems, is used here. A flexible implant shares more load with the periprosthetic bone, thereby limiting stress shielding and subsequent bone resorption [16–19]. However, a more flexible implant causes higher proximal interface stresses and motions [4,20]. In the unbonded case, increased motion may inhibit bone ingrowth [21,22] and in the bonded case, high interface stresses may disrupt fixation.

The design concept (Fig. 1) was characterized by two design factors: a reduced midstem diameter, d, and a bullet tip length, b. The total length of the implant remained fixed. Three environmental factors were also considered to contribute to the overall structural response: joint force angle (Θ), cancellous bone elastic modulus (E), and implant–bone interface friction (μ). The joint force angle was measured from a neutral or average joint force angle as determined in telemetric hip force studies [8] and thus described deviations from an expected joint force angle. The frequency of the (E_i,Θ_j) combinations (Fig. 2), was described by a discrete joint probability distribution, g_{ij}, to reflect in vivo variations. The robustness of the (b,d) design that was optimal with respect to the $\{g_{ij}\}$ distribution was investigated by considering several alternative distributions, also shown in Fig. 2. Rephrased, we asked whether the design that was optimal for the nominal distribution was also optimal for other distributions. Four of the alternative distributions (Fig. 2, bottom row) placed greater or less

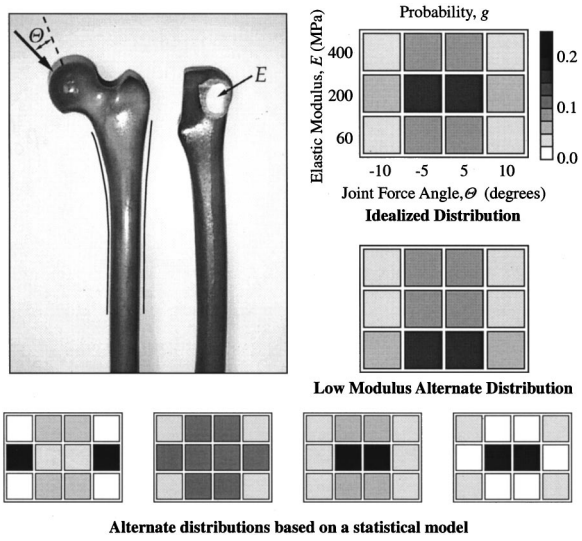

Fig. 2 Composite material analogs of an adult male femur (''Sawbones,'' Pacific Research Laboratories, Vashon, WA). The Sawbones, used in place of cadaver bones, consisted of an epoxy shell filled with polyurethane foam with one of three elastic moduli (E=60, 200, or 400 MPa). Also shown to the left is the definition of joint angle, Θ, meauserd from a neutral joint angle determined from a telemetric hip force study [8]. To the right, an idealized distribution, g, was assumed for the combinations of (E,Θ). Five alternate distributions are also displayed.

weight on extreme (E,Θ) combinations than the nominal distributions. A fifth alternative weighted lower values of cancellous bone elastic modulus, E, more heavily to idealize the distribution of a population of osteoporotic patients. A third environmental variable, interface friction, was described by a discrete uniform distribution of 10 points ranging from a frictionless interface, $\mu=0$, to an experimentally determined value for metal against bone, $\mu=0.42$ [23]. This range encompasses the conditions of a low-friction fibrous capsule formation around the implant to an immediate post-operative condition prior to bone ingrowth. Because interface friction is difficult to measure directly, one could consider the range as a means to account for modeling uncertainty where the true value falls somewhere within the maximum and minimum bounds.

The structural response, Y, was the absolute value of a bone remodeling signal [20] defined as the difference in strain energy density at location i in the intact femur (U_{oi}) and implanted femur (U_i),

$$Y=\sum_{i=1}^{m} \eta_i |U_{oi}-U_i| \tag{3}$$

where m was the total number of measurement sites in the bone and η_i was a weighting factor for location i. Strain energy density (J/mm^3) was measured at nodal locations on the bone surface along the periprosthetic medial and lateral aspects (Fig. 2) and each measurements site was weighted equally. A distinction was not made between a positive or negative remodeling signal, implying that both bone resorption and bone hypertrophy were considered undesirable. However, a negative bone remodeling signal (indicating the tendency for bone hypertrophy) was present in only a limited number of areas and did not affect the values for Y nor the overall results substantially.

A displacement constraint was imposed on the space of possible solutions. The tangential motion $(D_t=D_t(b,d,E,\Theta,\mu))$, averaged over the nodes in the proximal wedged region at the bone–implant interface, was constrained to be less than a limiting motion for bone ingrowth into porous surfaces,

$$\overline{D}_t \leqslant D_t^{\max}. \tag{4}$$

where $D_t^{\max}=50$ μm. Specifically, nodal relative motion $(\mathbf{d}_i)$ was calculated at each node on the proximal implant surface and was defined as the difference in absolute nodal displacements of the ith implant surface node and the bone surface node directly across the interface. The magnitude of tangential relative motion (D_t) between the stem and bone was averaged over all surface nodes on the proximal surface of the implant,

$$D_t=\frac{1}{n}\sum_{i=1}^{m} \|\mathbf{d}_i-(\mathbf{d}_i\cdot\hat{\mathbf{n}}_i)\hat{\mathbf{n}}_i\| \tag{5}$$

where n is the number of nodes and $\hat{\mathbf{n}}_i$ is the unit vector normal to the implant surface at the ith node.

Referring to Eqs. (1) and (2), the optimization formulation was

Minimize:

$$L(b,d)=\sum_i \sum_j \sum_k Y(b,d,E_i,\Theta_j,\mu_k)g_{ij}\frac{1}{10} \tag{6}$$

Subject to:

$$\overline{D}_t(b,d)=\sum_i \sum_j \sum_k D_t(b,d,E_i,\Theta_j,\mu_k)g_{ij}\frac{1}{10}\leqslant 50 \tag{7}$$

Here $\overline{D}_t(b,d)$ denotes the mean of D_t values over the same distribution for (E,Θ,μ). The optimization problem was solved approximately by substituting EBLUP's for Y and D_t in their respective mean formulas. For example, $\hat{Y}$ is substituted for Y in Eq. (6).

Bone–Implant System. The proximal implant was a cobalt chromium ($E_{CoCr}=220{,}000$ MPa) Ranawat-Burstein Implant (Biomet, Inc., Warsaw, IN) and the distal portion was modified to represent different combinations of the design variables (b,d) (Fig. 1).

The femoral geometry and material properties were from composite material analogs of the human femur (''Sawbones,'' Pacific Research Laboratories, Vashon WA) representing a medium to large male (Fig. 2). The average properties of the fiber composite representing cortical bone ($E_{\text{cort}}\cong 18{,}600$ MPa) and polyurethane foam representing cancellous bone ($E\cong 60$, 200, or 400 MPa), reported by Pacific Research Laboratories, were similar to those of real bone. A sawbones femur was used, instead of a cadaver femur, to provide a standard basis for comparison between different implant studies.

Computer Models. Three-dimensional nonlinear finite element models (Fig. 3) were developed using PATRAN (MSC, Costa Mesa CA). The bone–implant models consisted of 1352 20-noded brick or 15-noded wedge elements (5803 nodes). The implant was modeled as linearly elastic and isotropic with the properties of cobalt chrome. Bone properties were also assumed to be linearly elastic and isotropic but inhomogeneously distributed due to some variations in the manufacturing of the sawbones femurs. Material properties for bone were determined using CT scans of the sawbones femurs. Based on grayscale values and material properties reported by Pacific Research Labs, power laws were developed and elastic moduli were assigned to individual Gauss points. The elastic modulus assigned was either E_{cort}, E, or a very low modulus to simulate gaps between the bone and implant. The bone–implant interfaces were modeled with zero-tension Coulomb-friction interface elements with friction properties described by the uniformly distributed random variable $\mu\in[0,0.42]$.

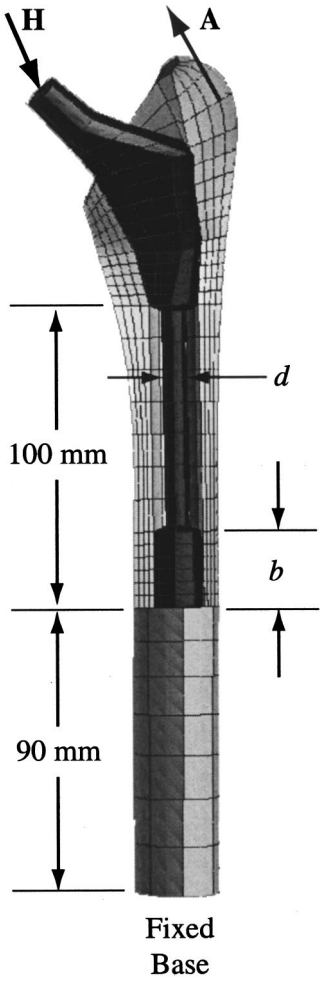

Fig. 3 Three-dimensional nonlinear finite element models. The implant was modeled as linearly elastic and isotropic with the properties of cobalt chrone (E_{CoCr}=220,000 MPa). Bone properties were also assumed to be linearly elastic and isotropic but with an inhomogeneous distribution. Material properties for bone were determined using CT scans of the Sawbones femurs. The bone–implant interfaces were modeled with zero-tension Coulomb-friction interface elements enabling an estimate of relative motion.

A hip contact force and an abductor muscle force (Fig. 3) were applied as point loads to the femoral head center and the greater trochanter, respectively. The nominal load acting on the femoral head (Table 1) was based on in vivo telemetric hip force measurements [7] and the greater trochanteric load was determined from a musculoskeletal model of a typical male patient and a muscle reduction analysis similar to Paul [24]. The proximal femur was truncated three bone diameters (90 mm) from the most distal aspect of each implant and fixed at its base in all directions. The models were solved using an in-house analysis software package (GNOME, Cornell University, Ithaca, NY). This software has been used with similar models described by Keaveny and Bartel [25].

Table 1 Nominal loading condition

	Axial (N)	Medial (N)
Joint Contact Force	−1770	−436
Abductor Muscle Force	844	488

All forces are expressed in Newtons for a 750 N patient. Two components of force are given for the two-dimensional beams on elastic foundation analysis.

Validation Experiment. Physical tests were performed on three intact composite material femurs (Pacific Research Laboratories, Vashon WA) and on the same femurs with implants to confirm the trends seen in the finite element models. The intact femurs were used as the baseline case for normalization of the bone remodeling signal. The truncated distal femurs were plotted in square aluminum channels using polyester body filler (NAPA, Cleveland OH, Cuz 6372). This left 90 mm between the top of the potting and the most distal portion of the prosthesis (when implanted). The femoral axis was held parallel to the square potting fixture. Three strain gage rosettes (Measurements Groups, Inc., Raleigh NC, Model EA-060125TM-120) were placed on both the medial and lateral sides of the bones. With the implant inserted, the gages were located 10 mm proximal to the implant's distal tip, 10 mm distal to the start of the reduced diameter section, and 30 mm proximal to the start of the reduced diameter section.

The instrumented femurs were mounted in an MTS-858 Mini Bionix servo-hydraulic tester. The fixture allowed for various head load angles by means of an angular vise (Fig. 4). A linear bearing contacted the femoral head to ensure that the load direction was strictly controlled by the vise angle. The abductor force was simulated by a cable attached to a rod inserted through the greater trochanter. The adjustable fixture coupled the head load and abductor load in such a way that the relative loading magnitudes in the computer models and the physical experiment were the same.

A cyclic ramp load, applied at 1 Hz and ranging from 10 to 100 percent of the finite element models' peak head load magnitude of 1825 N, was first applied with the femoral head and neck intact for each load angle in random order ($\Theta=\{-10,-5,5,10\}$deg). The prostheses were then implanted using a standard protocol under the supervision of an orthopaedic surgeon. The nine (b,d) combinations (Fig. 1) were tested in random order using separate random orders for each of the three femurs. For each of the (b,d)-femur combinations, the four load angles were also randomized. Prior to data collection, the specimens were conditioned for 30 cycles to allow the implant to settle.

The response predicted by the three-dimensional finite element models was compared with the physical experiments. For comparison, the bone remodeling response was recomputed with the finite element models at locations on the bone surface corresponding to strain gage locations in the physical experiments. Next, regression models were developed based on the physical experimental data to quantify the relative factor effects and to perform multiple comparisons between implant designs.

Results

Sequential Search Results. The second-stage predictor indicated that an optimal solution was contained in the lower-left quadrant of the original design space, corresponding to small values of bullet tip length and midstem diameter (Fig. 5). The third-stage predictor added six points restricted to the lower-left quadrant (a total of 22 training sites). The accuracy of prediction can be assessed by quantifying the associated prediction uncertainties. In general, there is greater certainty in areas more densely populated by training data. In the present study, the additional training points in the region containing the suspected minimum reduced the prediction error (Fig. 6) near the predicted optimum ($b=10$ mm, $d=7$ mm).

The predictor of the tangential motion constraint is shown in Fig. 7. The upper 95 percent prediction bound on tangential motion at the globally optimal design, $(b,d)=(10,7)$ was 50 μm, which was also the constraint value. Hence, the global optimum was the constrained optimum.

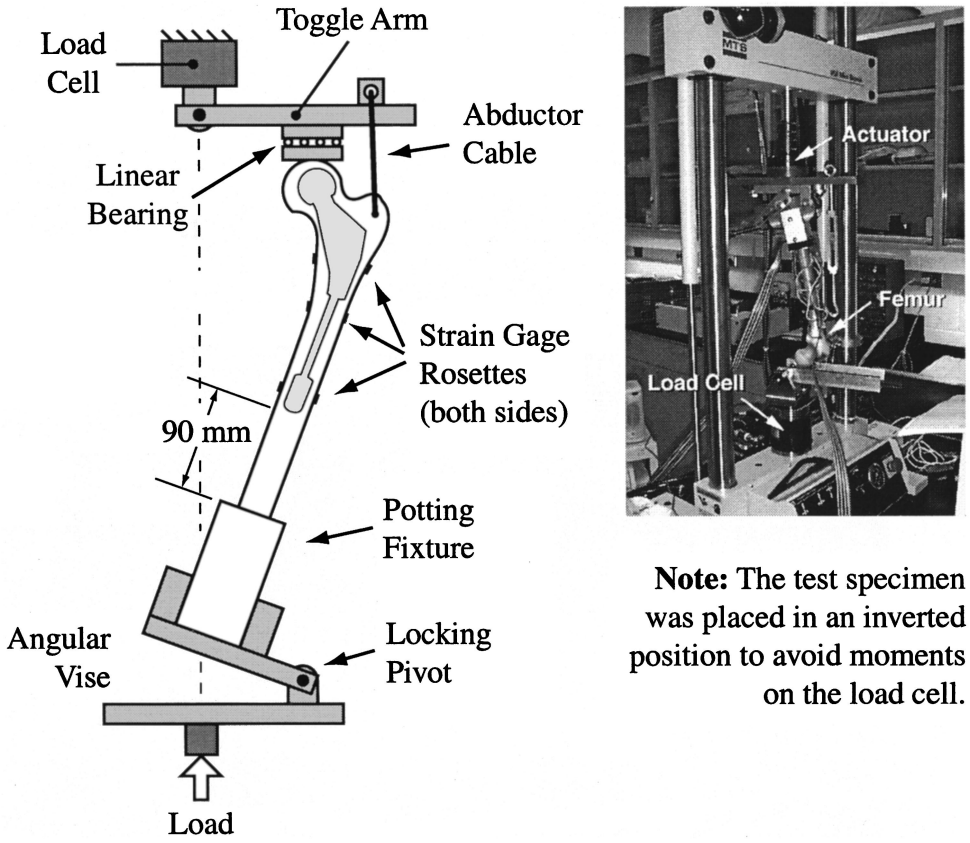

Fig. 4 Experimental test specimen and fixture schematic. Three strain gage rosettes were placed on both the medial and lateral sides of the bones. Load was applied with an MTS-858 Mini Bionix servohydraulic tester. The abductor force was simulated by a cable attached to a rod inserted through the greater trochanter. The adjustable fixture coupled the head load and abductor load in such a way that the relative loading magnitudes in the computer models and the physical experiment were the same.

Robustness of Optimal Design to Alternate Distributions. The design $(b,d)=(10,7)$ that was found to be optimum against the idealized environmental variable distribution was also optimal for a wide class of alternate distributions. The alternate distribution representing a low modulus distribution did alter the 95 percent upper prediction bound of tangential relative motion at the predicted optimum ($D_t^{95\%}(10,7)=53>50$ μm). To eliminate this constraint violation, an increased bullet tip length of greater than 20 mm was necessary while midstem diameter was maintained at 7 mm. This change did not significantly change the value of the objective function (Fig. 5).

Sensitivity Analysis. The factor contributions were predicted for the bone remodeling signal response, Y and for tangential motion constraint, D_t, based on the 22-point predictors (Fig. 8).

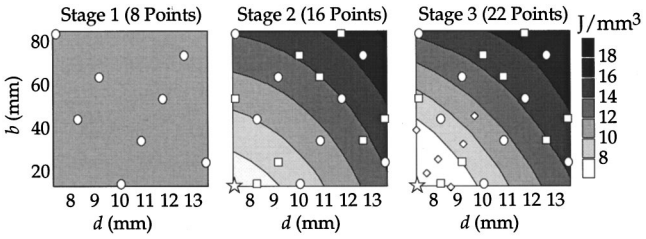

Fig. 5 The predicted objective function is presented for each stage of the optimal search. The *(b,d)* projections corresponding to the training sites are shown for the first-stage (8 circles), second-stage (8 circles plus 8 squares), and third-stage predictors (16 circles and squares plus 6 diamonds). Eight sites were insufficient to predict the effects of the design fabricators. The 16-point second-stage and third-stage predictors indicated an optimal design in the lower left quadrant of the design space corresponding to a minimal bullet tip length and midstem diameter. The predicted optimal (b,d) combination is denoted by a star.

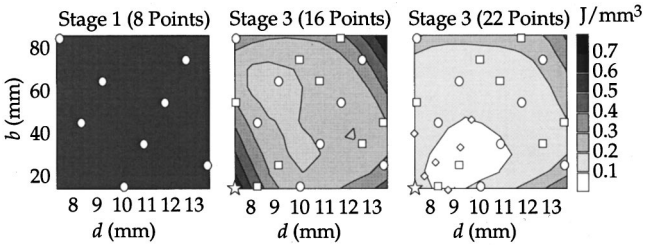

Fig. 6 The standard error of the objective function prediction is presented for each stage of the optimal search. The (b,d) projections corresponding to the training sites are shown for the first stage (8 circles), 16 point second-stage (8 circles plus 8 squares), and third-stage predictors (16 circles and squares plus 6 diamonds). Eight sites were insufficient to predict the effects of the design factors. The prediction error for the objective function diminished with increasing training sites. The third-stage predictor was specifically accurate in the region of objective function minima denoted by a star.

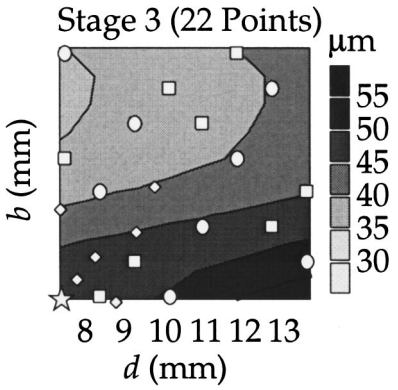

Fig. 7 The predicted tangential relative motion is presented for the third-stage training data

Interaction effects were generally small. The design factors had a relatively small effect on the bone remodeling signal compared with load angle, Θ, which accounted for 82 percent of the variation (Fig. 8). Cancellous bone modulus, E, and bone-implant interface friction, μ, had no effect on the bone remodeling signal.

The bullet tip length, b, accounted for 29 percent of the variation in tangential relative motion while the midstem diameter, d, had a relatively small effect (5 percent) (Fig. 8). Cancellous bone modulus was the dominant factor, explaining 50 percent of the variation in D_t.

Validation Experiment. Results from the three-dimensional finite element models indicated that bullet tip length and midstem diameter each contributed about 6 percent to overall variation in the bone remodeling signal. Revising the finite element models so that the remodeling signal was computed at the same set of measurement sites as the physical experiment showed that the predicted signal was essentially independent of bullet tip length and indicated an optimal midstem diameter of 7 mm. This was consistent with the measurements of the physical experiment (Fig. 9). In particular, 95 percent pairwise prediction intervals for the differences in the bone remodeling signal (averaged over the (E,Θ,μ) combinations) showed that the $d=7$ mm stems had significantly smaller values than either the $d=10$ or 13 mm stems.

Discussion

In the present study, we extended an efficient statistical optimization methodology previously introduced [9] by: (1) adding constraints explicitly into the formulation, (2) quantifying robustness to alternate distributions of the environmental variables, and (3) performing a sensitivity analysis to determine the relative importance of each factor.

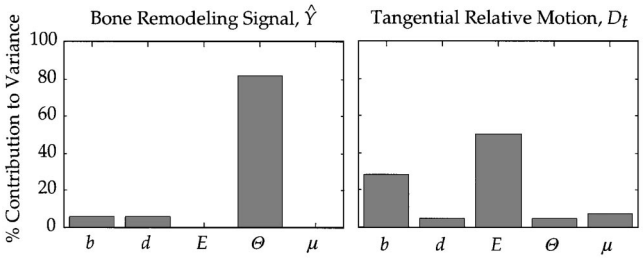

Fig. 8 Percent combination of factors. The main effects of design and environmental factors on the bone remodeling signal response function (Y) and tangential relative motion (D_t) are shown. Interaction effects were generally small. The percent contribution estimates are based on the third-stage (22-site) Latin hypercube sample.

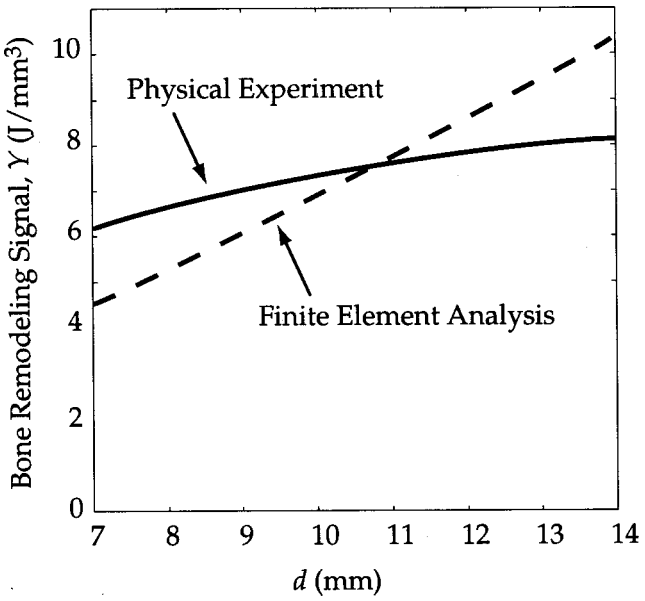

Fig. 9 Comparison of finite element predictions (averaged over values of bullet tip length, b) of the objective function with physical experiments. The predicted bone remodeling signal was re-computed from the finite element model results by considering strain energy density sites in the regions corresponding to strain gage placement in the physical experiments. Both results predict a minimum midstem diameter, $d=7$ mm. The effects of bullet tip length, b, were not presented because its contribution to the variation in the bone remodeling signal was approximately 1 percent.

The choice of total number of training sites and the breakdown of this total into sequential stages is heuristic. This is currently an active area of research [26]. Fortunately, the number of runs needed in this study is much fewer than for more traditional direct-search techniques and considerable leeway exists for exploration. For example, in the present study, only 22 finite element runs were needed to determine an optimal solution. For comparison, we counted the number of function evaluations required by a quasi-Newton direct search for the optimum using $\hat{L}(\mathbf{x_d})$ based on the 22 finite element training runs. This calculation provided a good estimate of the number of finite element runs that would have been needed using the direct search approach. With the inclusion of environmental variables, a typical search required on the order of 2000 function evaluations of Y, approximately 100 times the effort required using the statistical methodology.

Based on the 22-point predictor, a minimal bullet tip length and minimum midstem diameter design was optimal and was found to be on the boundary of the feasible region. For a population with lower cancellous bone moduli, more support was needed distally to satisfy the tangential motion constraint. This was most effectively achieved by increasing the length of the bullet tip.

Before discussing these findings further, it is important to discuss the limitations of the models employed so that any conclusions based on these simulations can be placed in the proper context. Two modeling choices were particularly influential on the predicted structural response: the use of composite femurs instead of cadaveric specimens, and the omission of out-of-plane loading.

CT images of the composite femurs do show a substantially thicker cortical shell in the metaphyseal region than for normal bone. Fortunately, the structural stiffness differences in the diaphysis, that is, in the region of implant design changes, were much less than in the metaphysis. These differences, compared with the stiffnesses of the range of intramedullary stems examined, would not have affected the general trends predicted if a cadaveric femur had been used. In addition to its effects on the bone remodeling

signal, the composite femur's thick cortical-like epoxy shell provided more resistance to relative motion because it provided more substantial contact points for the prosthesis. As a result, the predictions of relative motion were probably low. This should be noted when comparing the results of the present study with similar studies based on cadaver specimens or human subjects.

The composite femurs were modeled as continuous structures with linearly elastic material properties. Based on observations from physical experiments, the polyurethane foam collapsed in some regions during implantation and subsequent loading. This was not accounted for in the computer models and may have introduced additional error.

In-plane loading was considered in this study so that direct comparisons could be made with the beams on elastic foundation models of our previous study [9] and with the physical experimental results. Researchers [6,7] have shown that the out-of-plane component of force that causes a torsional moment can have a large influence on interface motion. The design variables considered in this study altered only the distal (cylindrical) portion of the implant and therefore did not substantially affect the implant's resistance to torsional loads. Therefore, the effects of the design changes on the bending response were appropriate and well predicted. Nevertheless, neglecting torsional moments resulted in low predictions of relative motion. The upper limit of 50 μm for tangential relative motion was conservatively small and therefore may have compensated for the low predictions of relative motion. Pilliar et al. [22] suggested that increased relative motion ($>$150 μm) could inhibit bone ingrowth and may promote formation of a fibrous tissue layer. However, this value is not appropriate for implant studies because motion was measured subsequent to bone ingrowth or fibrous capsule formation. Keaveny [27] described a mechanistic limit for micromotion based on the characteristic implant surface pore size. The range of pore sizes in the study by Pilliar et al. was 50 to 400 μm. Burke et al. [6] reported an average pore size of most implants between 200 and 300 μm. Based on these ranges, a conservative limit of $D_t^{\max}=50$ μm was imposed. For studies including the out-of-plane loading component, a more appropriate value may be on the order of 200 to 300 μm, the average pore size of most coated implants [6].

Trends from the physical experiments led to the same optimum as those computed using the finite element models when considering only those sites corresponding to the strain gage locations. In both cases, a minimum midstem diameter was predicted. In retrospect, the bullet tip length had a negligible effect on the bone remodeling signal due to the placement of a limited number of strain gage rosettes. Two of the rosettes were placed in areas of constant implant cross section and one was placed in a region that always had a midstem diameter reduction. As a result, only changes in midstem diameter were found to affect the response significantly.

The bone remodeling signal predicted with the three-dimensional finite element models agreed well with the corresponding predictions using one-dimensional beams on elastic foundation (BOEF) models used in our previous study [9]. This agreement provides evidence that the global response of the structure in bending is affected mostly by the relative stiffnesses of the implant and bone rather than by details at the interface coupling the two.

In addition to finding the optimal design, it may be equally beneficial to identify the specific factors that were most influential on achieving that optimal design. The results from the sensitivity analysis study can be useful in this respect. First, a 20 deg change in the joint force angle explained 80 percent of the variation in the bone remodeling signal. Second, cancellous bone elastic modulus and interface friction had no effect on the remodeling signal. The strain energy density at the surface of the bone was affected only by the global structural properties, that is, by the relative stiffnesses of the bone and implant. Cancellous bone modulus contributed negligibly to the femur's overall structural stiffness particularly in bending. In addition, the small interactions between the (b,d) and (E,Θ,μ) variables explains why $(b,d)=(10,7)$ mm combination is insensitive to alternative (E,Θ,μ) distributions. The surface $Y(b,d,E,\Theta,\mu)$ shows similar trends in the (b,d) space for all (E,Θ,μ).

The large effect of bullet tip length on tangential relative motion indicated that the increased frictional contact area in the diaphysis may have reduced the tendency for the implant to subside. Axial motion was indeed the major component of the tangential relative motion. This may also explain why the midstem diameter had a small effect on tangential motion. Cancellous bone elastic modulus was the most influential factor accounting for 50 percent of the variation in relative motion. Its influence was also apparent when considering the alternate distribution that represented an osteoporotic population. For this distribution, the bullet tip length had to be increased moderately from 10 mm to over 20 mm to compensate for the lack of support proximally in order to satisfy the tangential motion constraint.

Sensitivity analysis can be useful for identifying the relative impacts of design and environmental variables on the response. When there are a small number of variables, sensitivity analysis can be implemented by visual inspection of the response. In more complicated applications, sensitivity analysis will provide valuable insight and critical information for guiding the design of physical experiments to validate the computer model. By identifying a small number of influential variables, more focused experiments can be conducted.

The statistical methodology introduced in Chang et al. [9] and extended here is useful for determining optimal designs and understanding the behavior of implants with respect to multiple factors, and evaluating hypotheses resulting from clinical studies where many factors, design and environmental, are confounded. The example of a hip replacement was presented for illustrative purposes but the methods are obviously not restricted to this articulation. The knee joint, for example, is subjected to a more diverse set of loads in terms of position and orientation. Surgical preparation for and alignment of knee replacement components are also critical for proper kinematic function and load transfer. Therefore, future knee designs stand to benefit greatly from the application of these methods.

Acknowledgments

The authors thank Professor Marjolein van der Meulen for her advice and the use of her laboratory, and Joseph Lipman, Dr. Bruce Robie, Matthew Naimoli, and Dr. Brian Nestor for their assistance with experimental planning and specimen preparation. This study was supported by The Clark, Dana, and Frese Foundations, and the National Institutes of Health, Grant No. AR42737-01.

Nomenclature

b = bullet tip length
d = midstem diameter
$\mathbf{d}$ = relative interface motion vector
D_t = tangential relative motion between implant and bone
$\bar{D}_t$ = average tangential relative motion
E = cancellous bone elastic modulus
g = joint probability distribution for environmental variables
$\mathbf{h}$ = equality constraint function
L = objective function
$\hat{L}$ = predicted objective function
m = joint probability distribution for interface friction
U = strain energy density
U_o = strain energy density, intact femur
$\mathbf{x}$ = design and environmental variable vector $(\mathbf{x_d},\mathbf{x_e})$
$\mathbf{x_d}$ = design variable vector (b,d)
$\mathbf{x_e}$ = environmental variable vector (E,Θ)
Y = structural response

$\hat{Y}$ = predicted structural response
η = bone location weighting factor
μ = interface friction
Θ = joint force angular deviation
σ_z^2 = stochastic process variance

References

[1] Davy, D. T., and Katoozian, H., 1994, ''Three-Dimensional Shape Optimization of Femoral Components of Hip Prostheses With Frictional Interfaces,'' Trans. Annu. Meet.—Orthop. Res. Soc., **19**.

[2] de Beus, A. M., Hoeltzel, D. A., and Eftekhar, N. S., 1990, ''Design Optimization of a Prosthesis Stem Reinforcing Shell in Total Hip Arthroplasty,'' ASME J. Biomech. Eng., **112**, pp. 347–357.

[3] Huiskes, R., and Boeklagen, R., 1989, ''Mathematical Shape Optimization of Hip Prosthesis Design,'' J. Biomech., **22**, pp. 793–804.

[4] Kuiper, J. H., 1993, ''Numerical Optimization of Artificial Hip Joint Designs,'' Ph.D. Thesis, University of Nijmegen, The Netherlands.

[5] Yong, S. Y., Gun, H. J., and Young, Y. K., 1989, ''Shape Optimal Design of the Stem of a Cemented Hip Prosthesis to Minimize Stress Concentration in the Cement Layer,'' J. Biomech., **22**, pp. 1279–1284.

[6] Burke, D. W., O'Connor, D. O., Zalenski, E. B., Jasty, M., and Harris, W. H., 1991, ''Micromotion of Cemented and Uncemented Femoral Components,'' J. Bone Jt. Surg., Br. Vol., **73**, pp. 33–37.

[7] Kotzar, G. M., Davy, D. T., Berilla, J., and Goldberg, V. M., 1995, ''Torsional Loads in the Early Postoperative Period Following Total Hip Replacement,'' J. Orthop. Res., **13**, pp. 945–955.

[8] Noble, P. C., Alexander, J. W., Lindahl, L. J., Yew, D. T., and Granberry, W. M., 1988, ''The Anatomical Basis for Femoral Component Design,'' J. Orthop. Res., **235**, pp. 148–165.

[9] Chang, P. B., Williams, B. J., Santner, T. J., Notz, W. I., and Bartel, D. L., 1999, ''Robust Optimization of Total Joint Replacements Incorporating Environmental Variables,'' ASME J. Biomech. Eng., **121**, pp. 304–310.

[10] Bernardo, M. C., Buck, R., Liu, L., Nazaret, W. A., Sacks, J., and Welch, W. J., 1992, ''Integrated Circuit Design Optimization Using a Sequential Strategy,'' IEEE Trans. Comput.-Aided Des., **11**, pp. 361–372.

[11] McKay, M. D., Beckman, R. J., and Conover, W. J., 1979, ''A Comparison of Three Methods for Selecting Values of Input Variables in the Analysis of Output From a Computer Code,'' Technometrics, **21**, pp. 239–245.

[12] Sacks, J., Welch, W. J., Mitchell, T. J., and Wynn, H. P., 1989, ''Design and Analysis of Computer Experiments (With Discussion),'' Stat. Sci., **4**, pp. 409–435.

[13] Stein, M. L., 1999, *Interpolation of Spatial Data: Some Theory for Kriging*, Springer-Verlag, New York.

[14] Welch, W. J., Buck, R. J., Sacks, J., Wynn, H. P., Mitchell, T. J., and Morris, M. D., 1992, ''Screenign Predicting and Computer Experiments,'' Technometrics, **34**, pp. 15–25.

[15] Jones, D. R., Schonlau, M., and Welch, W. J., 1998, ''Efficient Global Optimization of Expensive Black-Box Functions,'' J. Global Optim., **13**, pp. 455–492.

[16] Bobyn, J. D., Mortimer, E. S., Glassman, A. H., Engh, C. A., Miller, J. E., and Brooks, C. E., 1992, ''Producing and Avoiding Stress Shielding, Laboratory and Clinical Observations of Noncemented Total Hip Arthroplasty,'' Clin. Orthop., **274**, pp. 79–96.

[17] Engh, C. A., and Bobyn, J. D., 1988, ''The Influence of Stem Size and Extent of Porous Coating on Femoral Bone Resorption After Primary Cementless Hip Arthroplasty,'' Clin. Orthop., **231**, pp. 7–28.

[18] Engh, C. A., McGovern, T. F., Bobyn, J. D., and Harris, W. H., 1992, ''A Quantitative Evaluation of Periprosthetic Bone Remodeling After Cementless Total Hip Arthroplasty,'' J. Bone Jt. Surg., Am. Vol., **77**, pp. 1009–1020.

[19] Sumner, D. R., Turner, T. M., Urban, R. M., and Galante, J. O., 1991, ''Experimental Studies of Bone Remodeling in Total Hip Arthroplasty,'' Clin. Orthop., **276**, pp. 83–90.

[20] Huiskes, R., Weinans, H., and van Rietbergen, B., 1992, ''The Relationship Between Stress Shielding and Bone Resorption Around Total Hip Stems and the Effects of Flexible Materials,'' Clin. Orthop., **274**, pp. 124–134.

[21] Karrholm, J., Borssen, B., Lowenhielm, G., and Snorrason, F., 1994, ''Does Early Micromotion of Femoral Stem Prostheses Matter? 4-7 Year Stereoradiographic Follow-up of 84 Cemented Prostheses,'' J. Bone Jt. Surg., Br., Vol. 1, **76**, pp. 912–917.

[22] Pilliar, R. M., Lee, J. M., and Maniatopoulos, C., 1986, ''Observations on the Effect of Movement on Bone Ingrowth Into Porous-Surfaced Implants,'' Clin. Orthop., **208**, pp. 108–113.

[23] Shirazi-Adl, A., Dammak, M., and Paiement, G., 1993, ''Experimental Determination of Friction Characteristics as the Trabecular Bone/Porous-Coated Metal Interface in Cementless Implants,'' J. Biomech., **27**, pp. 167–175.

[24] Paul, J. P., 1967, ''Forces at the Human Hip,'' Ph.D. Thesis, University of Glasgow, Scotland.

[25] Keaveny, T. M., and Bartel, D. L., 1993, ''Effects of Porous Coating, Wth and Without Collar Support, on Early Relative Motion for a Cementless Hip Prosthesis,'' J. Biomech., **26**, pp. 1355–1368.

[26] Williams, B. J., Santner, T. J., and Notz, W. I., 2000, ''Sequential Design of Computer Experiments to Minimize Integrated Response Functions,'' Statistical Sinica, in press.

[27] Keaveny, T. M., 1991, ''A Finite Element Analysis of Load Transfer and Relative Motion for Contemporary Cementless Hip Implants in the Short and Long-Terms,'' Ph.D. Thesis, Cornell University, Ithaca, NY.